# Multiplet effects on the shape of the 3*p* photoelectron spectrum of atomic Ni

K. Tiedtke, Ch. Gerth, B. Kanngießer, B. Obst, and P. Zimmermann
*Institut für Atomare und Analytische Physik, Technische Universität Berlin, Hardenbergstrasse 36, 10623 Berlin, Germany*

M. Martins
*Institut für Experimentalphysik, Freie Universität Berlin, Arnimallee 14, 14195 Berlin, Germany*

A. Tutay
*Physics Department, Istanbul University, 34459 Vezneciler, Istanbul, Turkey*

(Received 8 April 1999)

The $3p$ photoelectron spectrum and the corresponding $M_{2,3}$ Auger spectrum of atomic Ni have been measured with the use of monochromatized synchrotron radiation and atomic beam technique. The thresholds of the direct $3p$ photoionization have been determined. In order to interpret the complex $3p^{-1}$ multiplet structure calculations were performed taking into account the initial states of both configurations $3d^8 4s^2$ and $3d^9 4s$ and the $LS$-term dependence of the Ni $3p$ core-hole lifetimes. The strong influence of both the $3p$-$3d$ exchange interaction and the term dependent lifetime broadening by super-Coster-Kronig decays on the shape of the $3p$ photoelectron spectrum is demonstrated. [S1050-2947(99)03810-X]

PACS number(s): 32.80.Fb, 32.80.Hd

## I. INTRODUCTION

Core-level photoionization studies on $3d$ transition metals in the vacuum ultraviolet (vuv) region are of great interest in both the atomic and solid state communities (see [1] and references therein). With regard to the atomic side, the analysis of the complex $3p$ photoelectron spectra offers the possibility for critical tests of modern many-electron theories. The comparison of the atomic spectra with the corresponding solid-state spectra of metals, metal alloys, or metal compounds, on the other hand, yields essential information about the interplay of inter-atomic and intra-atomic interactions.

Ferromagnetic materials are of great practical importance and, thus, advanced experimental techniques like spin-polarized photoemission and linear and circular magnetic dichroism have been applied to investigate the solid-state $3p$ spectra in Fe, Co, and Ni (e.g., [2,3] and references therein). In the case of the atomic spectra these elements were studied by photoion- and photoelectron spectroscopy [4,5] with special emphasis on the region of the $3p$-$3d$ resonances between 50 and 80 eV. Due to the relatively weak cross sections, investigations on the direct $3p$ photoionization of atomic $3d$ transition metals, i.e., Cr [6], Mn [6–8], Fe [6,9], and Co [6], have only been made quite recently. The $3p$ photoelectron spectra exhibit a large multiplet splitting of about 20 eV [6,7], as a consequence of the strong coupling of the $3p$ core hole with the open $3d$ shell, and a small spin-orbit splitting of the $3p$ core hole [9]. Furthermore, the atomic character of the dichroism in the $3p$ photoionization of Cr has successfully been proven with laser-oriented Cr atoms [10]. Thus, a proper description of the $3p$ spectra of $3d$ transition metals requires the consideration of many-electron correlations.

This work reports on the $3p$ photoelectron spectrum of atomic Ni and, additionally, the corresponding $M_{2,3}$ Auger spectrum. For the production of a beam of free Ni atoms a high evaporation temperature of about 1800 K is required. As a consequence, the Ni spectra are more complicated than the spectra of Cr, Mn, Fe, and Co due to the fact that both initial-state configurations $3d^8 4s^2$ and $3d^9 4s$ are thermally populated. In order to analyze the complex multiplet structure, we performed Hartree-Fock (HF) calculations using the Cowan code [11]. The strong influence of both the $3p$-$3d$ electrostatic interaction and the term dependent lifetime broadening by super-Coster-Kronig (SCK) decays on the shape of the $3p$ photoelectron spectrum is demonstrated.

## II. EXPERIMENT

Our studies were carried out at the high-flux undulator beamline TGM5 at the electron storage ring BESSY I in Berlin (Germany). The synchrotron radiation was dispersed by a toroidal-grating monochromator and focused onto a beam of free atoms. For the production of the atomic beam we used an effusive oven heated by electron impact [12]. A temperature of about 1800 K was necessary for a sufficient particle density ($\approx 10^{11}$ cm$^{-3}$) in the interaction region of the atomic and the photon beam. At this elevated temperature Ni becomes an aggressive melt which alloys with refractory metals and, thus, Ni was contained in $Al_2O_3$ ceramics to avoid direct contact with the molybdenum crucible. Furthermore, initial states of both configurations $3d^8 4s^2$ and $3d^9 4s$ are thermally populated. The relative thermal population of these $3d^8 4s^2\ ^3F_J$ and $3d^9 4s\ ^3D_J$ states is summarized in Table I.

The kinetic energy of the photoelectrons emerging from the interaction region was measured with a SCIENTA SES 200 electron analyzer. All spectra were recorded at a fixed photon energy $h\nu$ by scanning the accelerating (retarding) lens voltage of the analyzer. The chosen analyzer pass energy of 75 eV resulted in a bandwidth of $\Delta E = 120 \pm 20$ meV constant over the whole spectrum. Only electrons with an angle of emission close to the magic angle of 54.7° relative to the polarization axis of the synchrotron radiation

 

TABLE I. Relative thermal population of the lowest Ni I states (notation of Ref. [18]) at an evaporation temperature of 1800 K.

| Config. | $(LSJ)$ | Energy (eV) | Rel. pop. (%) |
|---|---|---|---|
| $3d^8 4s^2$ | $^3F_4$ | 0 | 42 |
| | $^3F_3$ | 0.165 | 11 |
| | $^3F_2$ | 0.275 | 4 |
| $3d^9 4s$ | $^3D_3$ | 0.025 | 28 |
| | $^3D_2$ | 0.109 | 11 |
| | $^3D_1$ | 0.212 | 4 |

were accepted. All spectra were corrected for the analyzer transmission.

For intensity reasons a high photon flux was required and as a consequence a moderate experimental bandwidth (monochromator and electron analyzer) of 750 meV for the $3p$ photoelectron spectrum was achieved, while in the case of the Auger spectrum only the electron analyzer bandwidth of 120 meV accounted for the resolution. For the calibration of the monochromator and the energy scale of the electron analyzer we used well-known photoelectron and Auger lines of noble gases.

## III. EXPERIMENTAL AND THEORETICAL RESULTS

### A. 3p photoelectron spectrum

Figure 1 shows the $3p$ photoelectron spectrum of atomic Ni taken at a photon energy of 158.5 eV. The spectrum exhibits two prominent peaks at binding energies of approximately 73.0 eV ($A$) and 76.9 eV ($B$), a less intense structure between 79 and 86 eV ($C$) and a broad and suppressed structure $D$ in the high binding energy part of the spectrum.

For a more detailed analysis of the spectrum we performed HF calculations for an excitation energy of 150 eV using the Cowan code [11]. The HF values of the Slater integrals $F^k$ and $G^k$ were scaled down to 85%. The oscillator strengths of the transitions from the initial states into Ni $3p^{-1}\epsilon s,d$ final states were calculated; the different initial- and final-state configurations which were considered are summarized in Table II. The natural lifetimes of the

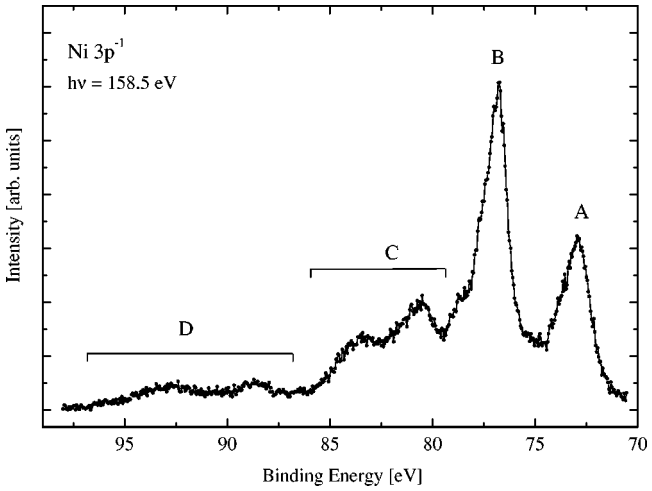


FIG. 1. $3p$ photoelectron spectrum of atomic Ni taken at a photon energy of 158.5 eV.

TABLE II. Initial and final state configurations included in the HF calculation of the $3p$ photoelectron spectrum.

| Initial-state configurations | Final-state configurations | |
|---|---|---|
| | Discrete | Continuum |
| $3p^6 3d^8 4s^2$ | $3p^5 3d^{10} 4s$ | $3p^5 3d^{10}\ \epsilon s,d$ |
| $3p^6 3d^9 4s$ | $3p^5 3d^9 4s^2$ | $3p^5 3d^9 4s\ \epsilon s,d$ |
| $3p^6 3d^{10}$ | $3p^5 3d^9 4p^2$ | $3p^5 3d^8 4s^2\ \epsilon s,d$ |
| $3p^6 3d^8 4p^2$ | | $3p^5 3d^8 4p^2\ \epsilon s,d$ |
| | | $3p^5 3d^8 4s 4d\ \epsilon s,d$ |
| | | $3p^5 3d^9 4d\ \epsilon s,d$ |

Ni II $3p^{-1}$ final ionic states were taken into account by calculating the transition rates of the subsequent Auger decays. We found out that these lifetimes show a strong $LS$-term dependence, which has a major effect on the spectral shape of the $3p$ photoelectron spectrum. The $3p$ photoelectron spectra calculated for the different thermally populated initial fine-structure states (see Table I) are depicted in panels (a)–(c) of Fig. 2. In addition to the term dependent lifetime, the instrumental broadening originating from the finite experimental resolution was taken into account by convoluting the spectra with a Gaussian profile (0.75 eV FWHM). The spec-

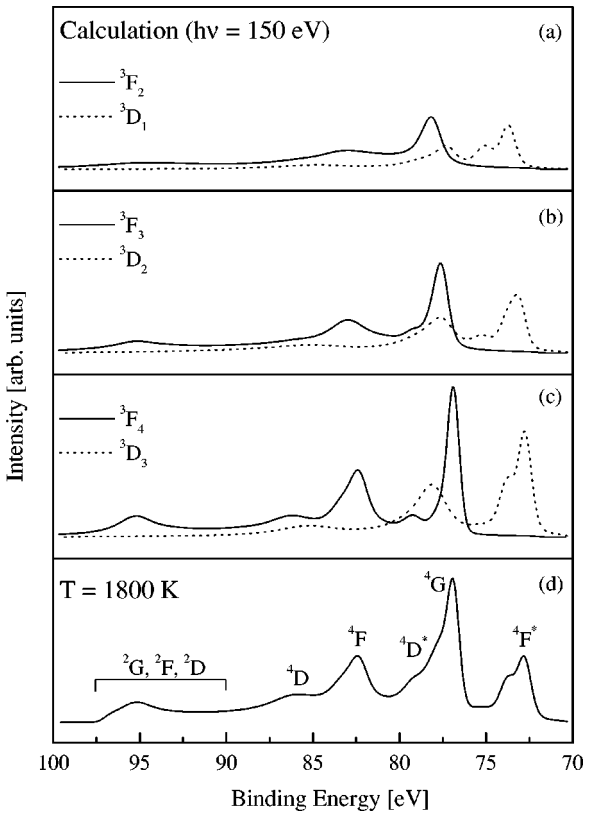


FIG. 2. (a)–(c) Calculated photoelectron spectra of the different fine-structure states. The energy scale of the contribution of the $^3F_J$ states (solid line) was shifted by $-0.8$ eV. The energy scale of the contribution of the $^3D_J$ states (dotted line) was shifted by $-2.4$ eV. (d) Sum of different fine-structure states weighted according to their thermal population (see Table I). Term-dependent lifetime broadening was taken into account and all spectra were convoluted with a Gaussian profile corresponding to the experimental resolution (0.75 eV FWHM).

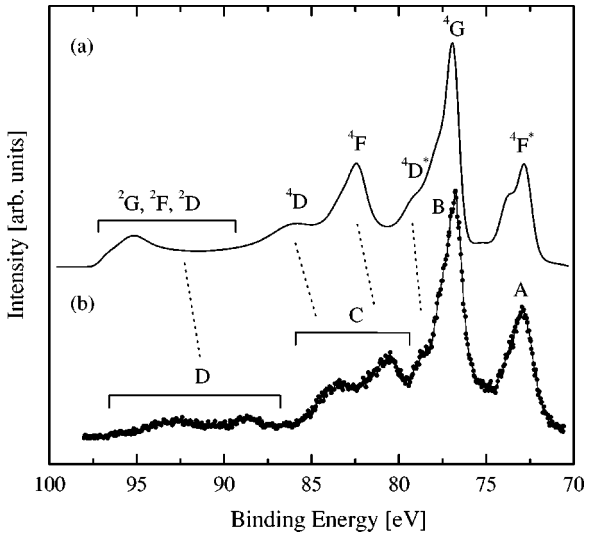


FIG. 3. Theoretical and experimental $3p$ photoelectron spectra of atomic Ni; (a) superposition of the spectra calculated for different thermally populated initial states [panel (d) of Fig. 2]; (b) experimental spectrum as shown in Fig. 1.

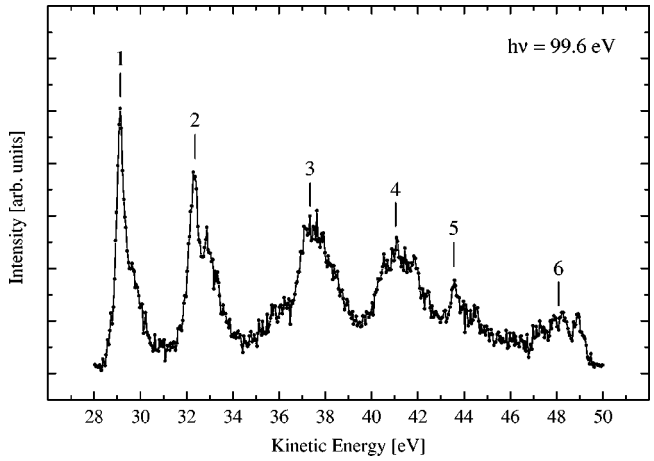


FIG. 4. $M_{2,3}$ Auger spectrum of atomic Ni taken at a photon energy of 99.6 eV.

tra calculated for the $3d^9 4s\ ^3D$ states (dotted lines) are quite similar to those of the $3d^8 4s^2\ ^3F$ states (solid lines) but located at lower binding energies. In order to obtain the best fit to the experimental photoelectron spectrum the energy scales for the contributions of the $^3F$ and $^3D$ states were shifted by $-0.8$ and $-2.4$ eV, respectively. This shifting is justified because the mismatch of energy positions of the states from different configurations is a common problem in HF calculations.

Figure 2(d) shows the superposition of the calculated spectra weighted according to the thermal population of the initial states. The prominent peaks are assigned to final ionic Ni II states, where the asterisks indicate those states which result from transitions from the $3d^9 4s\ ^3D_J$ initial states. The main contribution of these $^3D_J$ initial states to the final spectrum is the prominent $^4F^*$ peak, which represents the lowest Ni $3p$ ionization threshold.

From the two initial-state configurations $3d^8 4s^2\ ^3F$ and $3d^9 4s\ ^3D$ dipole transitions are allowed to $^2L$ low-spin states and $^4L$ high-spin states with $L=P,D,F,G$. The multiplet splitting extends over an energy range of 20 eV due to the large Slater integrals between the $3p$ and $3d$ electrons. The $3p$ photoelectron spectrum, thus, can be divided into a low binding energy and a high binding energy part. The high binding energy part, ranging from 90 to 97 eV, mainly consists of Ni II $3p^5 3d^8 4s^2\ ^2L$ low-spin states, which are considerably smeared out due to the strong lifetime broadening by intense SCK $3p$-$3d3d$ decays. The important role of the term dependence of the core-hole lifetimes was already pointed out by McGuire [13]. The more pronounced high-spin states are localized at binding energies between 72 and 87 eV. The spin-orbit splitting, being much smaller than the exchange splitting, was not resolved in our experiment.

The final curve of the calculation is depicted in Fig. 3 together with the experimental spectrum. The comparison shows that the spectral shape with the two main photoelectron lines ($A$ and $B$) in the low binding energy region of the spectrum, the large multiplet splitting, and the broadening of the low-spin states is well reproduced by the calculation. We assign the photoelectron lines observed experimentally to the following terms: Line $A$ at a binding energy of 73.0 eV can be ascribed to the $3d^9 4s\ ^3D \rightarrow 3p^5 3d^9 4s\ ^4F^*$ transition and corresponds to the lowest $3p$ ionization threshold. The experimental binding energy of 76.9 eV for the center of line $B$, which is primarily assigned to the Ni II $3p^5 3d^8 4s^2\ ^4D$ state, is in reasonable agreement with the value of 78.8(2.0) eV estimated from $M_{2,3}$ Auger spectra [14] excited by electron impact. Although the shape of the structure $C$ is not reproduced very well, we give a tentative assignment to the $^4D$ and $^4F$ final Ni II states according to the calculation. Correspondingly we assign the shoulder of line $B$ to the transition $3d^9 4s\ ^3D \rightarrow 3p^5 3d^9 4s\ ^4D^*$. The calculated $3p$ photoelectron spectrum predicts transitions from the $3d^8 4s^2\ ^3F$ to the $3d^8 4s^2\ ^2G$, $^2F$, $^2D$ low-spin states in the range of 90 to 97 eV. Therefore, we ascribe the broad structure $D$ to the $^2L$ states.

The spectral shape of the corresponding $3p$ photoelectron spectrum of $NiCl_2$ [15,16] differs from that of atomic Ni due to the hybridization between Ni $3d$ and Cl $3p$ orbitals. Nevertheless, the same strong influence of both the $3p$-$3d$ exchange interaction and the $LS$-term dependence of the $3p$ core-hole lifetime on the spectral shape was found. The strong coupling of the $3p$ core-hole with the open $3d$ shell leads to a large multiplet splitting of the order of 20 eV. The $3p$ core-hole states predominantly decay via $3p$-$3d3d$ SCK transitions; the lifetimes of the $3p$ core hole states strongly depend on the $LS$ terms. This $LS$-term dependence of the lifetime gives rise to the strong broadening of the low-spin states. The $M_{2,3}$ Auger spectrum of the high-spin states of atomic Ni will be discussed in more detail in the following chapter.

### B. $M_{2,3}$ Auger spectrum

Figure 4 shows the main Ni Auger lines, resulting from the decay of the $3p$ multiplet, excited at a photon energy of 99.6 eV. The spectrum displays four prominent Auger lines (1–4) in the range of 28 to 43 eV and two weak lines (5 and 6) centred at kinetic energies of $E_k = 43.6$ and 48.1 eV, respectively. Neglecting the small shoulder of line 1, we have fitted one Lorentzian profile to this Auger line. Taking into

TABLE III. Experimentally observed Ni Auger lines and their assignment together with the binding energies $E_b$ of the final Ni III states. The binding energies from Ref. [18] and the binding energies calculated are the weighted averages of various $J$ components of the Ni III final states. The uncertainty of the kinetic energies $E_k$ of the Auger lines amounts 0.2 eV.

| Auger | | Initial states | | Final states | | | |
|---|---|---|---|---|---|---|---|
| Line | $E_k$ (eV) | Ni II | $LS$ | Ni III | $LS$ | $E_b$ calculated (eV) | $E_b$ from [18] (eV) |
| 1 | 29.1 | $3p^5 3d^8 4s^2$ | $^4G$ | $3p^6 3d^6 4s^2$ | $^3H$ | 22.07 | |
| | | | | $3p^6 3d^6 4s^2$ | $^3P$ | 22.45 | |
| | | | | $3p^6 3d^6 4s^2$ | $^3F$ | 22.51 | |
| | | | | $3p^6 3d^6 4s^2$ | $^3G$ | 22.91 | |
| | | | | $3p^6 3d^6 4s^2$ | $^1I$ | 23.60 | |
| | | | | $3p^6 3d^6 4s^2$ | $^1G$ | 23.87 | |
| | | | | $3p^6 3d^6 4s^2$ | $^3D$ | 23.97 | |
| 2 | 32.3 | $3p^5 3d^8 4s^2$ | $^4G$ | $3p^6 3d^6 4s^2$ | $^5D$ | 19.10 | 19.10 |
| | | $3p^5 3d^9 4s$ | $^4F$ | $3p^6 3d^7$(b $^2$D)$4s$ | $^3D$ | 15.23 | 15.07 |
| | | | | $3p^6 3d^7$(b $^2$D)$4s$ | $^1D$ | 15.67 | 15.55 |
| 3 | 37.3 | $3p^5 3d^9 4s$ | $^4F$ | $3p^6 3d^7(^4P)4s$ | $^5P$ | 9.01 | 8.84 |
| | | | | $3p^6 3d^7(^2G)4s$ | $^3G$ | 9.26 | 9.37 |
| | | | | $3p^6 3d^7(^2G)4s$ | $^1G$ | 9.70 | 9.82 |
| | | | | $3p^6 3d^7(^4P)4s$ | $^3P$ | 9.85 | 9.72 |
| | | | | $3p^6 3d^7(^2P)4s$ | $^3P$ | 10.02 | 9.86 |
| | | | | $3p^6 3d^7(^2H)4s$ | $^3H$ | 10.03 | 10.19 |
| | | | | $3p^6 3d^7$(a $^2$D)$4s$ | $^3D$ | 10.28 | 10.23 |
| | | | | $3p^6 3d^7(^2F)4s$ | $^3F$ | 12.24 | 12.16 |
| | | | | $3p^6 3d^7(^2F)4s$ | $^1F$ | 12.68 | 12.64 |
| 4 | 41.1 | $3p^5 3d^9 4s$ | $^4F$ | $3p^6 3d^7(^4F)4s$ | $^5F$ | 6.80 | 6.80 |
| | | | | $3p^6 3d^7(^4F)4s$ | $^3F$ | 7.67 | 7.72 |

account the analyzer bandwidth of 120 meV a natural line width of 0.4(1) eV is obtained. Due to the quite similar energy spacing of the initial and final states, the different Auger decay channels overlap considerably and could not be resolved. For the assignment of the prominent Auger lines (1–4), given in Table III, we assume that the main contributions to these lines are due to $3p$-$3d3d$ SCK transitions from the $3p^5 3d^8 4s^2\,^4G$ and $3p^5 3d^9 4s\,^4F$ ionic states, which are denoted as lines $A$ and $B$ in Fig. 1. This assumption is well-founded as earlier investigations on the $3d$ transition metals Cr to Ni have shown: the Coster-Kronig (CK) and SCK transitions clearly dominate the decay of the $3p$ vacancy and, furthermore, the ratio of SCK to CK transition probability increases with atomic number $Z$ in the $3d$ transition metal series [14,17].

Because of the missing tabulated data of the energies of the $3d^6 4s^2$ Ni III levels, we performed HF calculations taking into account interaction between the configurations $3d^7 4s$, $3d^8$, and $3d^6 4p^2$. The calculated energy levels of the different configurations are shifted separately to give the best fit to the lowest tabulated value for each configuration.

According to the calculated Ni III $3d^6 4s^2$ energy levels we ascribe line 1 to the Ni II $3p^5 3d^8 4s^2\,^4G \rightarrow$Ni III $3d^6 4s^2 \epsilon l$ SCK decays. Earlier measurements of the $M_{2,3}$ Auger electrons of atomic Ni using electron beam excitation have detected only one Auger line with a kinetic energy of 34(2) eV [14], which is in reasonable agreement with the kinetic energy of line 2 in Fig. 4 at 32.3(2) eV. Correspondingly, Yin *et al.* [17] calculated the center of gravity for the kinetic energies of the Ni $M_{2,3}M_{4,5}M_{4,5}$ Augers of 31 eV. Unlike Ref. [14], we find that the subsequent $3p$-$3d3d$ SCK decay of both Ni II $3p^5 3d^8 4s^2\,^4G$ and Ni II $3p^5 3d^9 4s\,^4F$ states contribute to the second Auger line. Lines 3 and 4 can be related to predominant SCK processes of the $3p^5 3d^9 4s\,^4F$ hole states. In contrast to lines 1 and 2 with their relatively low kinetic energies, lines 3 and 4 can be superimposed by $3p$-$3d4s$ CK decays, which are energetically allowed, here, and beyond this, by SCK decay processes of the $3p^5 3d^8 4s^2\,^4D$, $^4F$ and $3p^5 3d^9 4s\,^4D$ states. A definite assignment for the lines 5 and 6 cannot be given due to the large number of energetically allowed transitions. However, these lines can be attributed to subsequent CK decay processes of the various $3p$ hole states denoted as line $A$ and $B$ and structure $C$ in Fig. 1.

## IV. SUMMARY

We have presented the direct $3p$ photoelectron spectrum of atomic Ni and the corresponding $M_{2,3}$ Auger spectrum. Due to the fact that both initial state configurations $3d^8 4s^2$ and $3d^9 4s$ are thermally populated at the evaporation temperature of 1800 K, the $3p$ photoelectron spectrum exhibits an elaborate multiplet structure. In order to interpret this complex $3p$ spectrum and to disentangle the contributions from both initial state configurations, we performed HF calculations taking into account the subsequent Auger decay of the Ni II $3p^{-1}$ multiplet states. The lifetimes of the Ni II $3p^{-1}$ multiplet states were found to be strongly term dependent. The $3p$-$3d$ electrostatic interaction and the $LS$-term

dependence of the lifetime considerably affect the spectral shape of the $3p$ photoelectron spectrum, which is dominated by a large multiplet splitting and a strong broadening of the low-spin states. The study of the $M_{2,3}$ Auger spectrum clarified that not only the subsequent decay of the low-spin states but also the deexcitation of the high-spin states can predominantly be attributed to $3p$-$3d3d$ SCK transitions.

**ACKNOWLEDGMENTS**

Many helpful discussions with Professor B. Sonntag, Universität Hamburg, are acknowledged with pleasure. The assistance of the BESSY staff is gratefully acknowledged. We are thankful for financial support from the Deutsche Forschungsgemeinschaft (Zi 183/12-1).

[1] B. Sonntag and P. Zimmermann, Rep. Prog. Phys. **55**, 911 (1992).
[2] T. Kachel, C. Carbone, and W. Gudat, Phys. Rev. B **47**, 15 391 (1993).
[3] J. G. Menchero, C. S. Fadley, G. Panaccione, F. Sirotti, and G. Rossi, Solid State Commun. **103**, 197 (1997).
[4] H. Feist, Ch. Gerth, M. Martins, P. Sladeczek, and P. Zimmermann, Phys. Rev. A **53**, 760 (1996).
[5] M. Meyer, Th. Prescher, E. von Raven, M. Richter, E. Schmidt, B. Sonntag, and H.-E. Wetzel, Z. Phys. D **2**, 347 (1986).
[6] A. von dem Borne, R. L. Johnson, B. Sonntag, M. Talkenberg, A. Verweyen, Ph. Wernet, J. Schulz, K. Tiedtke, Ch. Gerth, B. Obst, and P. Zimmerman (unpublished).
[7] J. Jiménez-Mier, M. O. Krause, P. Gerard, B. Hermsmeier, and C. S. Fadley, Phys. Rev. A **40**, 3712 (1989).
[8] S. Whitfield, M. O. Krause, P. van der Meulen, and C. D. Caldwell, Phys. Rev. A **50**, 1269 (1994).
[9] Ch. Gerth, K. Tiedtke, M. Martins, B. Obst, P. Zimmermann, P. Glatzel, A. Verweyen, Ph. Wernet, and B. Sonntag, J. Phys. B **31**, 2539 (1998).
[10] A. von dem Borne, T. Dohrmann, A. Verweyen, B. Sonntag, K. Godehusen, and P. Zimmermann, Phys. Rev. Lett. **78**, 4019 (1997).
[11] R. D. Cowan, *The Theory of Atomic Structure and Spectra* (University of California Press, Berkeley, CA, 1981).
[12] K. J. Ross and B. Sonntag, Rev. Sci. Instrum. **66**, 4409 (1995).
[13] M. E. McGuire, Phys. Rev. A **10**, 323 (1974).
[14] E. Schmidt, H. Schröder, B. Sonntag, H. Voss, and H.-E. Wetzel, J. Phys. B **17**, 707 (1984).
[15] M. Okusawa, Phys. Status Solidi A **124**, 673 (1984).
[16] K. Okada, A. Kotani, H. Ogasawara, Y. Seino, and B. T. Thole, Phys. Rev. B **47**, 6203 (1993).
[17] L. I. Yin, T. Adler, M. H. Chen, D. A. Ringers, and B. Crasemann, Phys. Rev. A **9**, 1070 (1974).
[18] J. Sugar and C. Corliss, J. Phys. Chem. Ref. Data Suppl. **14**, 407 (1985).